PHYSICAL REVIEW B **95**, 060402(R) (2017)

Evidence for a spinon Fermi surface in the triangular $S = 1$ quantum spin liquid $Ba_3NiSb_2O_9$

B. Fåk,[1,*] S. Bieri,[2,3,†] E. Canévet,[1,4,5] L. Messio,[3] C. Payen,[6] M. Viaud,[6] C. Guillot-Deudon,[6] C. Darie,[7] J. Ollivier,[1] and P. Mendels[8]

[1]*Institut Laue-Langevin, CS 20156, 38042 Grenoble Cedex 9, France*
[2]*Institute for Theoretical Physics, ETH Zürich, 8099 Zürich, Switzerland*
[3]*Laboratoire de Physique Théorique de la Matière Condensée, CNRS UMR 7600, Université Pierre et Marie Curie, Sorbonne Universités, 75252 Paris, France*
[4]*Laboratory for Neutron Scattering and Imaging, Paul Scherrer Institut, 5232 Villigen, Switzerland*
[5]*Laboratoire de Physique des Solides, Université Paris Sud 11, CNRS UMR 8502, 91405 Orsay, France*
[6]*Institut des Matériaux Jean Rouxel, CNRS UMR 6502, Université de Nantes, 44322 Nantes Cedex 3, France*
[7]*Institut Néel, CNRS, Univ. Grenoble Alpes, Boîte Postale 166, 38042 Grenoble Cedex, France*
[8]*Laboratoire de Physique des Solides, CNRS, Université Paris-Sud, Université Paris-Saclay, 91405 Orsay Cedex, France*

(Received 12 October 2016; published 1 February 2017)

Inelastic neutron scattering is used to study the low-energy magnetic excitations in the spin-1 triangular lattice of the $6H$-B phase of $Ba_3NiSb_2O_9$. We study two powder samples: $Ba_3NiSb_2O_9$ synthesized under high pressure and $Ba_{2.5}Sr_{0.5}NiSb_2O_9$ in which chemical pressure stabilizes the $6H$-B structure. The measured excitation spectra show broad gapless and nondispersive continua at characteristic wave vectors. Our data rules out most theoretical scenarios that have previously been proposed for this phase, and we find that it is well described by an exotic quantum spin liquid with three flavors of unpaired fermionic spinons, forming a large spinon Fermi surface.

DOI: 10.1103/PhysRevB.95.060402

Quantum spin liquids (QSLs) are exotic phases of condensed matter where the ground state evades ordering as a consequence of strong quantum fluctuations, frustration, or topological effects. QSLs are related to resonating-valence-bond states [1], and they exhibit fascinating properties such as long-range entanglement and fractional excitations [2–4]. The natures of such ground states are hotly debated questions, both in candidate materials [5–9] and in theoretical models [10–12], in particular concerning the existence of an excitation gap. Theoretically, a plethora of distinct and interesting possibilities for QSL phases has been classified [13–15]. To date, spin liquids have mainly been sought for in low-dimensional spin $S = 1/2$ systems, where quantum fluctuations are strongest. A pressing topic is therefore the existence of QSLs and their nature in systems with higher values of spin [16].

The $6H$-B phase of $Ba_3NiSb_2O_9$ [17] is of particular interest in this context. The Ni^{2+} ions form a frustrated triangular lattice of $S = 1$ spins. No sign of magnetic ordering is observed in the magnetic susceptibility down to $T = 2$ K [17], in the specific heat down to 0.35 K [17], or in muon spin rotation (μSR) measurements down to $T = 0.02$ K [18], while the Curie-Weiss constant of $\theta_{CW} = -76$ K indicates dominant antiferromagnetic interactions [17]. Strikingly, when $T \ll |\theta_{CW}|$, the compound shows a large linear term in the specific heat, $\gamma = 168$ mJ/mol K^2, and a finite magnetic susceptibility [17]. Such a metallic behavior in this strong Mott insulator suggests the presence of gapless coherent quasiparticles, possibly due to the emergence of a Fermi sea of fractional spinons. Evidence of gapless spin excitations are also found in recent NMR and μSR measurements [18].

Several scenarios have been discussed so far to explain the intriguing properties of $Ba_3NiSb_2O_9$. The $S = 1$ spin of the Ni^{2+} ions can be fractionalized into three [19] or four [20] fermionic spinons, resulting in rather different, but plausible QSL states: A chiral $\mathbb{Z}_2$ QSL with spinon Fermi surface [21,22] or a time-reversal symmetric $\mathbb{Z}_4$ QSL with quadratic spinon bands touching [20] have been proposed. Nematic three-dimensional spin liquids resulting from a bosonic fractionalization of spin have also been put forth [23]. Other proposals include the proximity to a quantum critical point as a consequence of fine-tuned inter- and intralayer exchanges, without the formation of a spin-liquid ground state [24].

In this Rapid Communication, we study powder samples of the $6H$-B structure of $Ba_3NiSb_2O_9$ using inelastic neutron scattering (INS) in order to bring clarity to these theoretical proposals. Broad gapless and nondispersive spin excitation continua are observed at three characteristic wave vectors. Strikingly, our wave-vector resolved data rule out most of the previous proposals for the magnetic low-temperature phase. We find that the INS data is well described by a U(1) quantum spin liquid with three flavors of spinons, forming a large spinon Fermi surface. This exotic spin $S = 1$ QSL state preserves full spin rotation and time-reversal symmetry, as well as all symmetries of the triangular lattice.

The $6H$-B phase of $Ba_3NiSb_2O_9$ reported in Ref. [17] crystallizes in the $P6_3mc$ space group with two Ni^{2+} ions at the $2b$ Wyckoff site, which form triangular layers of $S = 1$ spins with quenched orbital moments, stacked such that a Ni^{2+} ion in one layer sits above the center of the triangle formed by Ni^{2+} ions in the layer below. These layers are separated by nonmagnetic Sb layers, and appear well decoupled. We synthesized under pressure a 0.7 g powder sample of this $6H$-B phase of $Ba_3NiSb_2O_9$, as described in Ref. [25]. However, such a small quantity is hardly sufficient for detailed INS studies. We therefore made a larger 6.1 g powder sample of $Ba_{2.5}Sr_{0.5}NiSb_2O_9$, where chemical pressure via partial Ba/Sr substitution stabilizes the $6H$-B structure [26]. Rietveld

*fak@ill.fr
†samuel.bieri@alumni.epfl.ch

analyses of x-ray diffraction data from this $Ba_{2.5}Sr_{0.5}NiSb_2O_9$ sample collected at room temperature were performed using the published $P6_3mc$ or $P6_3/mmc$ crystal structures of $6H$-B $Ba_3NiSb_2O_9$ as a starting model [25]. As in pure $6H$-B $Ba_3NiSb_2O_9$, the best refinement was obtained for the $P6_3/mmc$ model [26]. The related structural questions, discussed in Ref. [25], concern essentially the stacking of the triangular layers, and are of little importance for the two-dimensional magnetic properties dealt with in the present work.

Our magnetic susceptibillity measurements of $Ba_{2.5}Sr_{0.5}NiSb_2O_9$ show an absence of magnetic order down to $T = 2$ K and a Curie-Weiss temperature of $\theta_{CW} = -80$ K [26], in close agreement with earlier measurements on $6H$-B $Ba_3NiSb_2O_9$ [17]. This suggests that the partial replacement of Ba with Sr does not change the magnetic properties of the compound. Assuming nearest-neighbor (NN) Heisenberg interactions, the Curie-Weiss temperature implies an antiferromagnetic NN exchange of $J_1 \sim 20$ K with the convention of counting each bond once.

The powder samples were put in an annular cylinder made from Cu or Al (depending on the temperature range) and thermalized by helium exchange gas. INS measurements were performed on the time-of-flight spectrometer IN5 at the Institut Laue-Langevin, using neutrons with several incident energies E_i between 1.13 and 20.4 meV at temperatures between 0.05 and 150 K using a dilution refrigerator or an orange cryostat. The energy resolution for elastic scattering follows approximately $\Delta E = 0.02(E_i)^{1.3}$ meV. Standard data reduction [27] including absorption corrections gave the neutron scattering function $S(Q,E)$, which is related to the imaginary part of the dynamic susceptibility via $\chi''(Q,E) = [1 - \exp(-E/k_BT)]S(Q,E)$ shown in Fig. 1. The data in this figure are not corrected for the magnetic form factor, and clearly illustrate that scattering from phonons is negligible in the energy and wave-vector range relevant for this work. Our neutron scattering data also show the absence of long-range magnetic order down to $T = 0.05$ K in $Ba_{2.5}Sr_{0.5}NiSb_2O_9$ and down to at least $T = 1.5$ K in $Ba_3NiSb_2O_9$.

The excitation spectrum shown in Fig. 1 is characteristic for a spin liquid, with vertical rods of broad scattering coming out at discrete wave vectors. The energy range of these excitations extends out to about 7.5 meV, which can be seen from both the Q and the temperature dependence of $S(Q,E)$ [see Fig. 2(a)]. The intensity extends down to energies below 0.04 meV [see Fig. 2(b)], i.e., they are gapless within the resolution of the present experiment. This is consistent with the large linear term in the specific heat [17] and the absence of a gap in NMR measurements of the spin-lattice relaxation rate $1/T_1$ [18]. Figure 2(c) shows the intrinsic energy dependence of the magnetic scattering

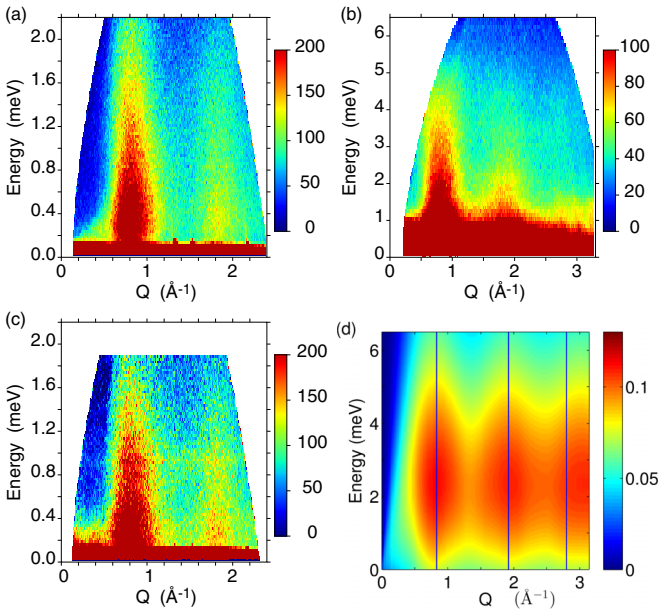

FIG. 1. Dynamic susceptibility $\chi''(Q,E)$ on a linear intensity scale as a function of wave vector Q and energy E at $T \approx 1.6$ K. (a) $Ba_{2.5}Sr_{0.5}NiSb_2O_9$ with an incoming neutron energy of $E_i = 3.55$ meV and (b) with $E_i = 8.0$ meV. (c) $Ba_3NiSb_2O_9$ with $E_i = 3.27$ meV (the weak feature at 1 meV is an experimental artifact). (d) Calculated powder-averaged $\chi''(Q,E)$ of the U(1) Fermi surface state (A) at 1/3 spinon filling (see text).

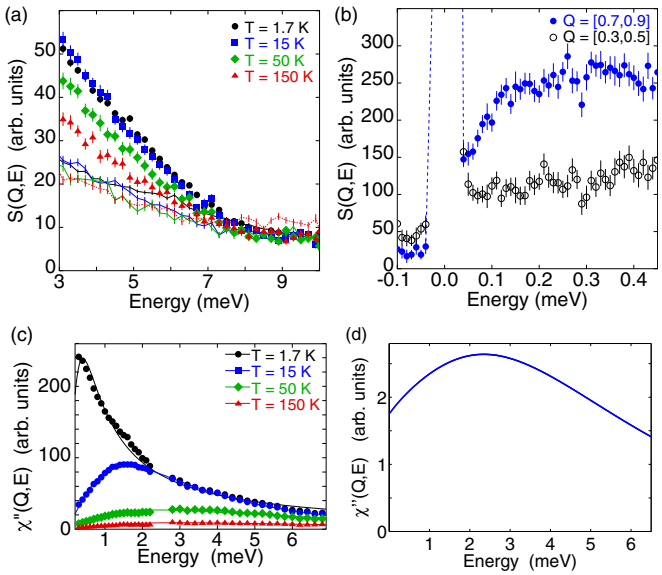

FIG. 2. (a)–(c) Energy dependence of the INS data from $Ba_{2.5}Sr_{0.5}NiSb_2O_9$. Panel (a) shows the temperature dependence of the dynamic structure factor $S(Q,E)$ at wave vectors $Q = 1.9 \pm 0.1$ Å^{-1} (magnetic signal, symbols) and $Q = 3.7 \pm 0.1$ Å^{-1} (mostly nonmagnetic signal, lines) measured with an incoming neutron energy of $E_i = 14.2$ meV. The excitations extend out to an energy of about 7.5 meV. Panel (b) shows $S(Q,E)$ at $Q = 0.8 \pm 0.1$ Å^{-1} (magnetic signal, solid blue circles) and $Q = 0.4 \pm 0.1$ Å^{-1} (mostly nonmagnetic signal, open black circles) for $T = 0.1$ K measured with $E_i = 1.13$ meV. The excitations are gapless within the experimental energy resolution (the dashed lines indicate the extension of the elastic peak). Panel (c) shows the imaginary part of the dynamic susceptibility $\chi''(Q,E)$ at $Q = 0.8 \pm 0.1$ Å^{-1} for different temperatures obtained by combining data obtained with $E_i = 3.55$ and 14.2 meV. The lines are guides to the eye. (d) Theoretical susceptibility at $Q \simeq 0.8$ Å^{-1} for the U(1) Fermi surface state at $T = 0$.

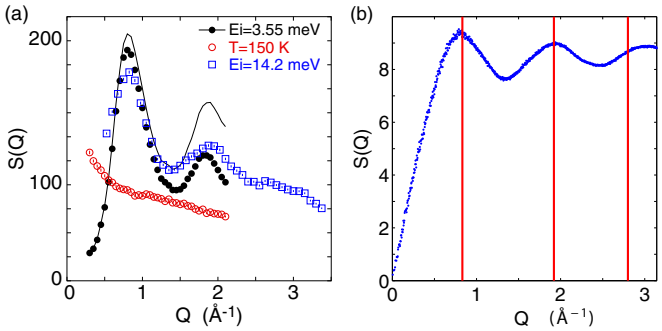

FIG. 3. (a) Q dependence of $S(Q,E)$ of $Ba_{2.5}Sr_{0.5}NiSb_2O_9$ at $T = 1.5$ K integrated over the energy range 0.3–1.5 meV at $E_i = 3.55$ meV (solid black circles) and 2–4 meV at $E_i = 14.2$ meV (open blue squares) showing peaks at $Q = 0.83$ and 1.92 Å^{-1}. The black line shows the $T = 1.5$ K data taken at $E_i = 3.55$ meV and corrected for the magnetic form factor. The open red circles show data taken with $E_i = 3.55$ meV at $T = 150$ K, where most of the correlations have disappeared. (b) Calculated static structure factor $S(Q)$ for the U(1) Fermi surface state (A) at $T = 0$.

$\chi''(Q,E)$ (i.e., without Bose factor) at $Q = 0.8 \pm 0.1$ Å^{-1} for different temperatures. The characteristic energy [peak position of $\chi''(Q,E)$] increases and the intensity decreases with increasing temperature.

The wave-vector dependence of the scattering after integration over a finite energy interval is shown in Fig. 3(a). At low temperatures, the spin-liquid scattering peaks at wave vectors $Q_1 = 0.83$ and $Q_2 = 1.92$ Å^{-1}, with a third broad peak at $Q_3 = 2.8$ Å^{-1}. The data taken with a higher incoming energy is slightly broader due to a wider range for the energy integration. The correlations in Q persist up to at least $T = 50$ K (not shown), which confirms the low-dimensional (here, two-dimensional) nature of the magnetic scattering. At even higher temperatures, $T = 150$ K, the correlations have almost completely disappeared [red open circles in Fig. 3(a)]. The height of the second peak in $S(Q)$ at $Q_2 = 1.92$ Å^{-1} is reduced with respect to the first one, even after correction for the magnetic form factor of the Ni^{2+} ions [see black line in Fig. 3(a)]. Attempts to fit the observed structure of $S(Q)$ using broadened Bragg peaks are found to fail. As we will discuss below, the peaks in $S(Q)$ can be attributed to extended regions of reciprocal space, i.e., strong intensity rings close to the boundary of the two-dimensional Brillouin zone (BZ).

INS measurements were also performed on the pressure synthesized $Ba_3NiSb_2O_9$ powder sample. Despite the usage of a high-flux low-resolution configuration with an incoming energy of $E_i = 3.27$ meV, the limited sample quantity led to a strongly reduced statistical quality of the data. Within the precision of these measurements, no major differences were observed compared to the $Ba_{2.5}Sr_{0.5}NiSb_2O_9$ sample [see Fig. 1(c)], which makes us confident that the experimental data on the latter are representative of the triangular $6H$-B lattice of $Ba_3NiSb_2O_9$.

To make further progress, we calculate the static and dynamical spin structure factors for a large number of pertinent gapless quantum spin-liquid states for spin $S = 1$ on the triangular lattice. For this, we use fractionalization of spin into three [19] and four [20] flavors of fermionic spinons. We primarily perform these calculations at the mean-field level, i.e., in the unconstrained Hilbert space, but we have checked that Gutzwiller projection only weakly renormalizes the static susceptibilities and spinon spectra in the relevant cases. More specifically, we investigate three classes of QSLs: (A) the U(1) state with three spinons forming a large Fermi sea discussed in [22], (B) the $\mathbb{Z}_4$ QSL with quadratic band touching (QBT) of four spinons proposed in Ref. [20], and (C) a generalization of the recently constructed Dirac spin liquid for triangular spin $S = 1/2$ systems [15,28–30] to spin $S = 1$ and three spinons, resulting in a state with small spinon Fermi pockets. Other theoretical proposals for this material are either inconsistent with the gapless and diffuse nature of the measured spin structure factor, and/or are ruled out by the indication of unbroken spin rotation symmetry in recent NMR and μSR measurements [18].

The QSL scenarios (A)–(C) have a set of natural parameters that can be related to microscopic spin models. For the Fermi-surface states (A) and (C), we adjust the relative fillings of the three spinons, due to a potential single-ion anisotropy term D [21,22]. In the QBT state (B), we add a second-neighbor mean field, related to interaction on that bond.

Among the considered families of states, we find only (A) to be consistent with the INS data. The QSL families (B) and (C) show intensity maxima and minima in their powder-averaged structure factors that are inconsistent with experiment [26]. For state (A), the agreement is best when all spinons have an approximately equal filling of 1/3, indicating the absence of a sizable D term and unbroken spin-rotation symmetry in the material. The calculated powder-averaged spin structure factor is shown in Fig. 1(d). It exhibits broad spinon continua at three wave vectors, extending down to zero energy, consistent with the INS data displayed in the other panels. In Fig. 2(d), we plot an energy cut of the calculated intensity, integrated over the maximum at $Q = 0.8 \pm 0.1$. The strong low-energy weight and "belly shape" of this curve are consistent with experiment. However, the intensity is skewed towards high energy, probably due to unphysical components in the mean-field wave function. This may be corrected by invoking Gutzwiller projection removing spinon double occupancies [31–33], or by incorporating gauge fluctuations that mediate spinon interaction [34]. Such calculations are beyond the scope of this work [35].

We also calculate the bandwidth of Gutzwiller-projected two-spinon excitations in state (A) [36–38]. Assuming a short-range spin model, we estimated $W \simeq 4J$, where J is the microscopic exchange energy. Using the bandwidth measured in INS, we conclude that $J \simeq 22$ K, in surprisingly good agreement with the observed Curie-Weiss temperature. This energy scale is used in Figs. 1(d) and 2(d). For noninteracting spinons, the corresponding hopping amplitude is $t \simeq 16$ K, leading to a large linear term in the specific heat of $\gamma \simeq 0.18\pi^2/t \simeq 0.11$ K^{-1} at 1/3 filling of spinons. Furthermore, the Wilson ratio is $R_W = 8/3 \simeq 2.7$. These values deviate from the experimental ones ($\gamma^{\text{expt.}} = 0.02$ K^{-1}, $R_W^{\text{expt.}} = 5.6$ [17]), which, to some extent, is due to the neglect of spinon interactions in our crude estimates.

The energy-integrated (static) spin structure factor of state (A) is shown in Fig. 3(b), along with the corresponding

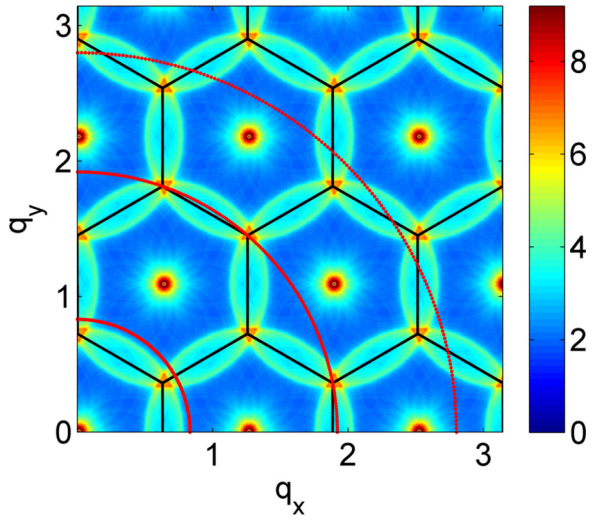

FIG. 4. Dynamical susceptibility $\chi''(q,E)$, energy integrated from 0 to 5% of the spinon band width, in the U(1) Fermi surface state (A) at 1/3 spinon filling. The black hexagons are the BZ boundaries, and the radii of the red circles centered at Γ correspond to the three broad intensity maxima seen in the INS data.

experimental data in the left panel. The vertical red lines indicate the positions of the measured INS maxima. In Fig. 4, we show the low-energy dynamical spin susceptibility of state (A) in two-dimensional momentum space of the triangular lattice. The BZ boundaries are shown as black hexagons. The continua at the Γ points come from $q \sim 0$ two-spinon excitations, while the broad intensities close to the BZ boundary are due to the $q \sim 2k_F$ excitations of the large spinon Fermi surface. The red circles indicate the Q momenta of the experimental intensity rods seen in INS. The powder average of the intensity in Fig. 4, assuming negligible dispersion in the third direction, is shown in Fig. 1(d). This averaging [26] has two crucial effects: First, the broad intensity maxima are slightly shifted to larger Q, such that the $2k_F$ features in Fig. 4 accurately reproduce the locations of the INS maxima. Second, the $q \sim 0$ intensities close to Γ are washed out and absorbed in a broad background.

The microscopic origin of QSL (A) is not fully understood. The state is known to have a low (but not lowest) variational energy [21,22] in a nearest-neighbor Heisenberg model with strong biquadratic interaction [39–41]. A three-site ring exchange term can further stabilize it, but then a triplet pairing sets in, resulting in a chiral $\mathbb{Z}_2$ QSL phase [21,22]. Another approach [42] found that a four-site ring exchange term can stabilize phase (A). We hope our results will stimulate further theoretical work on microscopic mechanisms.

In conclusion, we used inelastic neutron scattering to investigate the magnetic excitation spectrum of powder samples of the 6H-B phase of $Ba_3NiSb_2O_9$. Broad gapless and nondispersive excitation continua are observed at characteristic wave vectors. Comparing with several plausible theoretical models, we find that the low-temperature phase realized in this spin $S = 1$ Mott insulator is best described by a state of three flavors of unpaired fermionic spinons, and the observed spectrum is consistent with the $2k_F$ continua of a large two-dimensional spinon Fermi surface.

This work was supported in part by the French Agence Nationale de la Recherche, Grant No. ANR-12-BS04-0021. The inelastic neutron scattering experiments were performed at the Institut Laue-Langevin (ILL) in Grenoble. S.B. acknowledges the hospitality and support of the ILL and the International Institute of Physics at the Universidade Federal do Rio Grande do Norte, Brazil. We thank B. Bernu, F. Bert, M. Enderle, P. A. Lee, C. Lhuillier, and J. A. Quilliam for helpful discussions.

[1] P. W. Anderson, G. Baskaran, Z. Zou, and T. Hsu, Phys. Rev. Lett. **58**, 2790 (1987).
[2] L. Balents, Nature (London) **464**, 199 (2010); P. A. Lee, Science **321**, 1306 (2008).
[3] R. Moessner and A. P. Ramirez, Phys. Today **59** (2), 24 (2006).
[4] P. Mendels and F. Bert, C. R. Phys. **17**, 455 (2016).
[5] T.-H. Han, J. S. Helton, S. Chu, D. G. Nocera, J. A. Rodriguez-Rivera, C. Broholm, and Y. S. Lee, Nature (London) **492**, 406 (2012).
[6] B. Fåk, E. Kermarrec, L. Messio, B. Bernu, C. Lhuillier, F. Bert, P. Mendels, B. Koteswararao, F. Bouquet, J. Ollivier, A. D. Hillier, A. Amato, R. H. Colman, and A. S. Wills, Phys. Rev. Lett. **109**, 037208 (2012).
[7] Y. Shimizu, K. Miyagawa, K. Kanoda, M. Maesato, and G. Saito, Phys. Rev. Lett. **91**, 107001 (2003).
[8] Y. Shimizu, H. Akimoto, H. Tsujii, A. Tajima, and R. Kato, J. Phys.: Condens. Matter **19**, 145240 (2007).
[9] M. Fu, T. Imai, T.-H. Han, and Y. S. Lee, Science **350**, 655 (2015).
[10] A. M. Läuchli, J. Sudan, and E. S. Sørensen, Phys. Rev. B **83**, 212401 (2011).
[11] S. Depenbrock, I. P. McCulloch, and U. Schollwöck, Phys. Rev. Lett. **109**, 067201 (2012).
[12] Y. Iqbal, F. Becca, S. Sorella, and D. Poilblanc, Phys. Rev. B **87**, 060405 (2013).
[13] X.-G. Wen, Phys. Rev. B **65**, 165113 (2002).
[14] L. Messio, C. Lhuillier, and G. Misguich, Phys. Rev. B **87**, 125127 (2013).
[15] S. Bieri, C. Lhuillier, and L. Messio, Phys. Rev. B **93**, 094437 (2016).
[16] Z.-X. Liu, Y. Zhou, and T.-K. Ng, Phys. Rev. B **82**, 144422 (2010).
[17] J. G. Cheng, G. Li, L. Balicas, J. S. Zhou, J. B. Goodenough, C. Xu, and H. D. Zhou, Phys. Rev. Lett. **107**, 197204 (2011).
[18] J. A. Quilliam, F. Bert, A. Manseau, C. Darie, C. Guillot-Deudon, C. Payen, C. Baines, A. Amato, and P. Mendels, Phys. Rev. B **93**, 214432 (2016).
[19] Z.-X. Liu, Y. Zhou, and T.-K. Ng, Phys. Rev. B **81**, 224417 (2010).
[20] C. Xu, F. Wang, Y. Qi, L. Balents, and M. P. A. Fisher, Phys. Rev. Lett. **108**, 087204 (2012).

[21] M. Serbyn, T. Senthil, and P. A. Lee, Phys. Rev. B **84**, 180403 (2011); **88**, 024419 (2013).
[22] S. Bieri, M. Serbyn, T. Senthil, and P. A. Lee, Phys. Rev. B **86**, 224409 (2012).
[23] K. Hwang, T. Dodds, S. Bhattacharjee, and Y. B. Kim, Phys. Rev. B **87**, 235103 (2013).
[24] G. Chen, M. Hermele, and L. Radzihovsky, Phys. Rev. Lett. **109**, 016402 (2012).
[25] C. Darie, C. Lepoittevin, H. Klein, S. Kodjikian, P. Bordet, C. V. Colin, O. I. Lebedev, C. Deudon, and C. Payen, J. Solid State Chem. **237**, 166 (2016).
[26] See Supplemental Material at http://link.aps.org/supplemental/10.1103/PhysRevB.95.060402 for further details on sample preparation and characterization as well as on theoretical results. Additional references in the Supplemental Material are [43–48].
[27] LAMP, http://www.ill.fr/data_treat/lamp.
[28] Y.-M. Lu, Phys. Rev. B **93**, 165113 (2016).
[29] W. Zheng, J.-W. Mei, and Y. Qi, arXiv:1505.05351.
[30] Y. Iqbal, W.-J. Hu, R. Thomale, D. Poilblanc, and F. Becca, Phys. Rev. B **93**, 144411 (2016).
[31] J.-W. Mei and X.-G. Wen, arXiv:1507.03007.
[32] B. Dalla Piazza, M. Mourigal, N. B. Christensen, G. J. Nilsen, P. Tregenna-Piggott, T. G. Perring, M. Enderle, D. F. McMorrow, D. A. Ivanov, and H. M. Rønnow, Nat. Phys. **11**, 62 (2015).
[33] S. Bieri and D. A. Ivanov, Phys. Rev. B **75**, 035104 (2007).
[34] O. I. Motrunich, Phys. Rev. B **72**, 045105 (2005).
[35] In the calculated dynamical susceptibilities [Figs. 1(d), 2(d), and 4], we use a spinon lifetime broadening $\Gamma \sim |\omega|^{2/3}$, as suggested by coupling to a U(1) gauge field [49]. This broadens the intensity and moves it down in energy, but it does not affect the main conclusions of this work.
[36] S. Bieri, L. Messio, B. Bernu, and C. Lhuillier, Phys. Rev. B **92**, 060407 (2015).
[37] M. Hermele, Y. Ran, P. A. Lee, and X.-G. Wen, Phys. Rev. B **77**, 224413 (2008).
[38] Theoretically, we define the bandwidth by taking a spinon from the Fermi surface to an outermost level. Spin excitations constructed taking spinon states from far below to far above the Fermi energy are expected to be strongly suppressed. See also [26].
[39] A. Läuchli, F. Mila, and K. Penc, Phys. Rev. Lett. **97**, 087205 (2006).
[40] M. Moreno-Cardoner, H. Perrin, S. Paganelli, G. De Chiara, and A. Sanpera, Phys. Rev. B **90**, 144409 (2014).
[41] A. Völl and S. Wessel, Phys. Rev. B **91**, 165128 (2015).
[42] H.-H. Lai, Phys. Rev. B **87**, 205131 (2013).
[43] V. Petříček, M. Dušek, and L. Palatinus, Z. Kristallogr.-Crystalline Materials **229**, 345 (2014).
[44] G. A. Bain and J. F. Berry, J. Chem. Educ. **85**, 532 (2008).
[45] J. A. M. Paddison, M. Daum, Z. Dun, G. Ehlers, Y. Liu, M. B. Stone, H. Zhou, and M. Mourigal, Nat. Phys. (2016), doi: 10.1038/nphys3971.
[46] T. Li and F. Yang, Phys. Rev. B **81**, 214509 (2010).
[47] F. Tan and Q.-H. Wang, Phys. Rev. Lett. **100**, 117004 (2008).
[48] L. Messio, C. Lhuillier, and G. Misguich, Phys. Rev. B **83**, 184401 (2011).
[49] S.-S. Lee, Phys. Rev. B **80**, 165102 (2009).